X-Ray Diffraction Structures of Some Phosphatidylethanolamine Lamellar and Inverted Hexagonal Phases*

Paul E. Harper,[‡] David A. Mannock,[†] Ruthven N. A. H. Lewis,[†] Ronald N. McElhaney,[†] and Sol M. Gruner[‡]

[†]Department of Biochemistry, University of Alberta, Edmonton, Alberta T6G 2H7, Canada and [‡]Department of Physics, Princeton University, Princeton, New Jersey 05844, USA

ABSTRACT   X-ray diffraction is used to solve the low-resolution structures of fully hydrated aqueous dispersions of seven different diacyl phosphatidylethanolamines (PEs) whose hydrocarbon chains have the same effective chain length but whose structures vary widely. Both the lower-temperature, liquid-crystalline lamellar (L_α) and the higher-temperature, inverted hexagonal (H_{II}) phase structures are solved, and the resultant internal dimensions (d-spacing, water layer thickness, average lipid length, and headgroup area at the lipid–water interface) of each phase are determined as a function of temperature. The magnitude of the L_α and H_{II} phase d-spacings on either side of the L_α/H_{II} phase transition temperature (T_h) depends significantly on the structure of the PE hydrocarbon chains. The L_α phase d-spacings range from 51.2 to 56.4 Å, whereas those of the H_{II} phase range from 74.9 to 82.7 Å. These new results differ from our earlier measurements of these PEs (Lewis et al., *Biochemistry*, 28:541–548, 1989), which found near constant d-spacings of 52.5 and 77.0–78.0 Å for the L_α and H_{II} phases, respectively. In both phases, the d-spacings decrease with increasing temperature independent of chain structure, but, in both phases, the rate of decrease in the L_α phase is smaller than that in the H_{II} phase. A detailed molecular description of the L_α/H_{II} phase transition in these PEs is also presented.

INTRODUCTION

A complete understanding of the physical properties of specific membrane lipids requires a determination of the phase structures that are formed by these lipids under defined conditions. Because the lipid phases of biological interest are fully hydrated liquid–crystal mesophases, such a structural measurement involves a determination of the electron density distribution of the lipid/water system from a small number of powder-pattern-averaged orders of x-ray diffraction. In this article, we describe such a structure determination method that is then applied to aqueous dispersions of various phosphatidylethanolamines (PEs). In an accompanying article to be published elsewhere (D. A. Mannock, R. N. A. H. Lewis, R. N. McElhaney, P. E. Harper, and S. M. Gruner, submitted for publication), these results will be used in a comparative study of PEs and diacyl-α-D-glucosyl-glycerols containing fatty acyl chains of various lengths and structures.

To illuminate the physical principles at work in these systems, it is important to study systems with a variety of chemical structures to differentiate between general physical behavior and physical behavior that varies with the lipid chemical structure. In this paper, we determine the structural parameters of seven PEs with hydrocarbon chains having different chemical structures, but the same effective chain length (ECL).

The ECL of a hydrocarbon chain is defined by the total number of carbons in the "main chain." For linear saturated and unsaturated fatty acyl groups, the ECL equals the total number of carbon atoms present, whereas for the branched fatty acyl chains, the ECLs equal the total number of carbon atoms minus those present in the branch(es). For ω-cyclohexyl fatty acyl groups, where three carbon atoms of the terminal six-membered ring actually form part of the main chain, the ECL is equal to the total number of carbon atoms present minus three.

Although the unit cell basis vector lengths (d-spacings) of both the lamellar liquid-crystalline (L_α) and inverted hexagonal phases (H_{II}) are readily measured, additional information about the specific chemical structures of these lipids may be used to compute the electron density reconstructions to determine such quantities as average lipid length ($\langle l \rangle$) and water layer thickness (w and r). We first detail the theory and practice of this method of performing the reconstructions and then apply the method to various PEs. The results presented here also serve to correct earlier measurements (Lewis et al., 1989), in which some of the structural dimensions versus temperature were incorrect by as much as 10% due to a faulty temperature calibration arising from a voltage bias in the temperature controller.

MATERIALS

The seven PEs used in this study were 1,2-di-O-[*cis*-9,10-octadecenoyl-("oleoyl")]-3-O-phosphatidylethanolamine-*sn*-glycerol (18:1*c*Δ9-PE), 1,2-di-O-[*trans*-9,10-octadecenoyl("elaidoyl")]-3-O-phosphatidylethanol-amine-*sn*-glycerol (18:1*t*Δ9-PE), 1,2-di-O-[16′-ethyl-octadecanoyl]-3-

TABLE 1 Measured volumes of the hydrocarbons used to calculate the volumes of the diacyl phosphatidylethanol-amines in Table 2

Hydrocarbon	Formula	Density (gm/cm^3)	Volume (Å^3)
n-Octane	C_8H_{18}	0.6985	271.7
n-Nonane	C_9H_{20}	0.7138	298.6
n-Decane	$C_{10}H_{22}$	0.7262	325.5
2-Methyl decane	$C_{11}H_{24}$	0.7330	354.3
3-Methyl decane	$C_{11}H_{24}$	0.7396	351.3
3-Ethyl nonane	$C_{11}H_{24}$	0.7493	346.6
2,2-Dimethyl nonane	$C_{11}H_{24}$	0.7314	355.1
cis-2-Octene	C_8H_{16}	0.7202	258.9
trans-2-Octene	C_8H_{16}	0.7157	260.5
n-Hexylcyclohexane	$C_{12}H_{24}$	0.8041	347.8

Atomic weights of 12.01 for carbon and 1.01 for hydrogen were used to calculate the lipid molecular weights (Handbook of Chemistry and Physics). Densities were taken from the American Petroleum Institute Research Project 44. All values were measured at 25°C.

O-phosphatidylethanolamine-*sn*-glycerol (20:0$_{eai}$-PE), 1,2-di-O-[17′,17′-dimethyl-octadecanoyl]-3-O-phosphatidylethanolamine-*sn*-glycerol (20:0$_{dmi}$-PE), 1,2-di-O-[16′-methyl-octadecanoyl]-3-O-phosphatidylethanolamine-*sn*-glycerol (19:0$_{ai}$-PE), 1,2-di-O-[15-cyclohexyl-pentadecanoyl]-3-O-phosphatidylethanolamine-*sn*-glycerol (21:0$_{ch}$-PE), and 1,2-di-O-[17′-methyl-octadecanoyl]-3-O-phosphatidylethanolamine-*sn*-glycerol (19:0$_i$-PE). The numbers in the above abbreviated chemical nomenclature indicate the total number of carbon atoms in the hydrocarbon chain and the number, configuration, and position of any double bonds in the chain, whereas the subscripts indicate the type and position of the branches in the hydrocarbon chain (Lewis et al., 1989). The 18:1cΔ9-PE and 18:1tΔ9-PE were purchased from Avanti Polar Lipids (Alabaster, AL) and used as received. The remaining lipids were synthesized as described earlier (Lewis et al., 1989).

METHODS

Lipid molecular volumes

To determine the structural parameters of the various PEs studied, estimations of their molecular volumes are required. The volumes of 18:1cΔ9-PE and 18:1tΔ9-PE as a function of temperature and pressure have been measured by a combination of the method of neutral buoyancy in H_2O/D_2O mixtures (Nagle and Wilkinson, 1978) and high-pressure dilatometry (So et al., 1992). These methods require >100 mg of lipid, which is much more than the available supply of the other 18 carbon ECL PEs. Alternatively, the molecular volumes of the lipids can be estimated to the required accuracy by using the volumes of similar constituent hydrocarbons (see Table 1), along with the measured value for 18:1cΔ9-PE and the assumption that the headgroup volumes of all the PEs are identical. For the temperature dependence, it is known that lipids like 18:1cΔ9-PE and 18:1tΔ9-PE in their L_α phases have a coefficient of expansion of $\Delta V/V = 7 \times 10^{-4}/°C$ and that the L_α/H_{II} phase transition involves a $\Delta V/V$ of approximately 0.33% (So, 1992). Therefore, if the volume of a lipid is known at one temperature, the linear approximation given above can be used to determine the volume at any other temperature in the L_α portion of the phase diagram to an accuracy of better than 1% (So, 1992; So et al., 1993).

As a specific example and as a test of the accuracy of such an estimation, consider the two PCs for which the specific volumes are known, 15:0$_i$-PC (1.01 ml/g at 45°C; Yang et al., 1986) and 16:0-PC (1.004 ml/g

TABLE 2 Estimated volumes for several 18-carbon atom ECL hydrocarbon chain structural variants of diacyl phosphatidylethanolamine

Lipid	Volume (Å^3) Measured	Volume (Å^3) Estimated	18:1cΔ9-PE + 2(octane − *cis*-2-octene + X)*
18:1cΔ9-PE	1279[†]	–	N/A
16-ethyl-PE	–	1407	3-ethyl nonane − nonane
18:1tΔ9-PE	1258[‡]	1281	*trans*-2-octene − octane
20:0$_{dmi}$-PE	–	1425	2,2-dimethyl nonane − nonane
19:0$_{ai}$-PE	–	1360	3-methyl decane − decane
21:0$_{ch}$-PE	–	1409	*n*-hexylcyclohexane − nonane
19:0$_i$-PE	–	1366	2-methyl decane − decane

All calculated values are estimates of molecular volumes at a temperature of 100°C and are accurate to ±2%.
*X is the measured volume of fragments calculated from Table 1.
[†]The volume for 18:1cΔ9-PE has been calculated from the measurement obtained at 25°C by Tate and Gruner (1989) using the coefficient of thermal expansion from the work of So and co-workers. The remaining lipid molecular volumes, except for 18:1tΔ9-PE, were calculated using the values for the hydrocarbons shown in Table 1 and were adjusted from 25°C to 100°C using a coefficient of thermal expansion of $\Delta V/V = 7 \times 10^{-4}/°C$ (So, 1992). See text for details.
[‡]So, 1992.

at 45°C; Melchior et al., 1980). The molecular weights of 15:0$_i$-PC and 16:0-PC are 762.11 and 734.05, respectively, yielding volumes of 1278 and 1224 Å^3, respectively. We can estimate the specific volume of 15:0$_i$-PC, $v_{15i\text{-PC}}$, by considering it to be the volume

$$v_{15i\text{-PC}} = v_{16:0\text{-PC}} + 2(v_{2\text{-methyl-decane}} - v_{n\text{-decane}})$$

$$= 1224 \text{ Å}^3 + 2(359 - 330 \text{ Å}^3) = 1282 \text{ Å}^3,$$

which is in good agreement with the measured value of 1278 Å^3. A similar calculation for 18:1tΔ9-PE, starting from the measured value of 18:1cΔ9-PE, yields a value that is within 2% of the measured value for 18:1tΔ9-PE. Volumes for the other lipids are evaluated similarly and are presented in Table 2.

General electron density reconstruction theory

Our concern is with the L_α and the H_{II} phases, both of which are centrosymmetric. If one has a centrosymmetric unit cell (i.e., $\rho_e(\mathbf{r}) = \rho_e(-\mathbf{r})$, where ρ is the electron density and $\mathbf{r}$ is the vector to the position in the unit cell), the electron density can be written as a Fourier series of cosines. With A_q being the Fourier coefficients and q the Fourier vector, the electron density, ρ_e, as function of position $\mathbf{r}$ can be written,

$$\rho_e(\mathbf{r}) = \rho_{avg} + \sum_q A_q \cos(\mathbf{q} \cdot \mathbf{r}), \qquad (1)$$

where ρ_{avg} is the average electron density. For a powder sample of crystals, one will see a pattern of concentric rings of diffraction, each ring corresponding to a Fourier component q of the electron density. The integrated intensity I_q of a ring is related to its Fourier coefficient A_q by

$$I_q \propto \frac{mA_q^2}{\sin \theta} \approx \frac{mA_q^2}{\theta}, \qquad (1a)$$

where m is the multiplicity factor for the coefficient and the sin θ factor is the Lorentz correction (see Warren, 1969). The multiplicity is the number

of orientations of a crystal relative to the incoming x-rays that will yield a given reflection. The approximation $\sin \theta \approx \theta$ is made because all data are in the small angle region, $\theta < 0.1$.

In the small angle regime, the Lorentz correction (up to an overall scaling factor) is made by dividing the integrated intensities of the diffraction orders by the magnitude of the reciprocal lattice vector. For instance, the intensity of the second-order peak in the L$_\alpha$ phase is divided by 2. In the H$_{II}$ phase, the reciprocal lattice vectors also form a hexagonal lattice, and so, from geometry, the magnitude of the vector (h, k) is $\sqrt{(h^2 + hk + k^2)}$. Therefore, the $(1, 1)$ peak in the H$_{II}$ phase is divided by $\sqrt{3}$. (For more information on the Lorentz correction, see Warren (1969) and Turner (1990)). The peak intensity is divided by the multiplicity of the reflection. For example, in the H$_{II}$ phase, the $(1, 0)$ peak has the same magnitude and reciprocal vector length as the $(0, 1)$, $(1, -1)$, $(-1, 1)$, $(-1, 0)$, and $(0, -1)$ peaks, and so has a multiplicity of 6. Therefore, the peak intensity of $(1, 0)$ peak is divided by 6. For the L$_\alpha$ phase, all the peaks have a multiplicity of 1. For the H$_{II}$ phase, the peaks $(2, 1)$, $(3, 1)$, $(3, 2)$, and $(4, 1)$ each have a multiplicity of 12 and the remaining peaks have a multiplicity of 6 (Turner, 1990).

This is almost enough information to reconstruct the electron density of the liquid crystals from x-ray diffraction. What is missing are the signs of the A_q, e.g., the relative phases of the diffracted orders. Several methods have been developed to deal with this difficulty. One method is to construct a model of the electron density consistent with a known lipid chemical structure and then to pick the phasing that comes closest to reproducing the model, subject to the constraint that the rejected choices are clearly unphysical. Conversely, one can Fourier transform the model and then use the resulting phases in the reconstruction. Extensive work in modeling lamellar structures has been done by Wiener et al. (1992) and the H$_{II}$ structure has been modeled by Turner and Gruner (1992). Another means to determine the phases is the swelling method, in which structures at slightly different hydrations are compared. Because the electron density should only be shifted slightly by a small change in hydration, it is a reasonable assumption that the integrated difference of the square of the electron densities should be at a minimum for the proper phasing. This method was used by Stamatoff and Krimm (1976) for lamellar systems and was extended to H$_{II}$ systems by Turner (1990) and Turner and Gruner (1992). Yet another method is the $\langle \rho_e^4 \rangle$ technique of Luzzati and co-workers, where ρ_e is the electron density. They stated that, if one compares two structures of identical chemical composition, the value of $\langle \rho_e^4 \rangle$ should be the same for both. If one structure has a known phasing, this can be used to determine the phasing for the other structure. A recent example of this method is contained in Mariani et al. (1990). A new phasing technique, the methyl trough search, has recently been described by our groups (Harper and Gruner, 2000; Harper et al., 2000).

Lamellar phase reconstruction

A first step in determining a proper phasing for the L$_\alpha$ system is to construct a simple model of what a correct phasing should yield, based on an estimate of the molecular volume for each of the seven PEs studied here. These volumes were estimated by assuming that all of the PE polar headgroups have a single invariant volume and that the acyl chain volume may be estimated from known molecular volumes of the "constituent" hydrocarbons, as described above. The hydrocarbons that were used are listed in Table 1 and the estimated lipid molecular volumes are given in Table 2.

18:1$c\Delta$9-PE may be used as an example of the treatment of each of the seven lipids: The volume of 18:1$c\Delta$9-PE is 1190 Å at 25°C (Tate and Gruner, 1989). The methyls on the two hydrocarbon chains occupy a total of 2×56 Å$^3 = 112$ Å^3, or about 10% of the lipid volume. There are a total of 18 electrons in the methyl groups, yielding an electron density of 0.16 e/Å^3. The volume of the methylene portion of chains minus the terminal methyls can be estimated by comparison to the known molecular volumes of the constituent hydrocarbons measured at 25°C shown in Table 1,
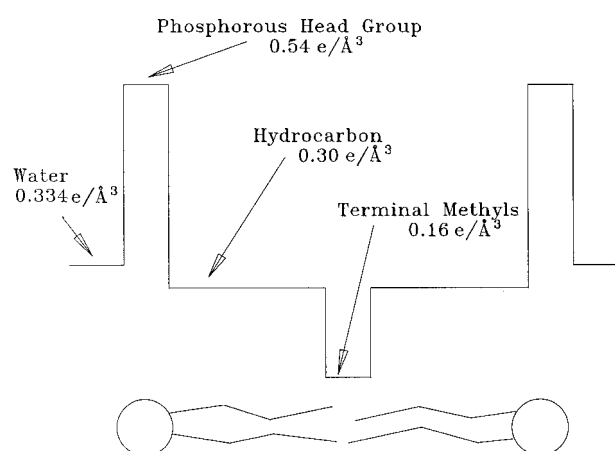

FIGURE 1 Electron density model of the L$_\alpha$ phase for 18:1$c\Delta$9-PE.

$$
\begin{aligned}
v_{\text{chains-methyls}} &= 2 \times (16 v_{\text{CH}_2} - v_{\text{n-octane}} + v_{\text{cis-2-octene}}) \\
&= 2 \times (16[v_{\text{n-nonane}} - v_{\text{n-octane}}] - v_{\text{n-octane}} \\
&\qquad\qquad\qquad\qquad\qquad + v_{\text{cis-2-octene}}) \\
&= 835.2 \ \text{Å}^3.
\end{aligned} \tag{2}
$$

From Eq. 2, it is seen that the hydrocarbon chains minus the methyl groups occupy about 70% of the lipid volume and that the remaining 20% is taken up by the headgroup. From the chemical composition of 18:1$c\Delta$9-PE, it is a simple matter to calculate the electron densities for these regions, which are 0.30 e/Å^3 for the hydrocarbon chains and 0.54 e/Å^3 for the polar headgroup. A diagram of this simple model is shown in Fig. 1. The model illustrates the basic features of a correct reconstruction, namely a methyl trough bounded by the headgroup peaks, which give way to the water region, which is of intermediate electron density. Note that this model is appropriate to all of the lipids under study here except for 21:0$_{\text{ch}}$-PE, which has no terminal methyls. Because there is no methyl trough for 21:0$_{\text{ch}}$-PE, the electron density in the tail region should be fairly flat.

For the L$_\alpha$ phase, the electron density is given by

$$
\rho_{\text{lam}}(\mathbf{r}) = \rho_{\text{avg}} + \sum_{i=1}^{\infty} A_i \cos\left(\frac{2\pi i x}{d}\right), \tag{3}
$$

where d is the repeat spacing of the crystal and x is in a direction perpendicular to the membrane surface. The ρ_{avg} cannot be determined from the reflection data alone, and may be set to zero for the reconstructions on an arbitrary electron density scale.

Inverted hexagonal phase reconstruction

A method of Turner and Gruner (1992) was used to reconstruct the H$_{II}$ phase. This technique is based on earlier work by Stamatoff and Krimm (1976), who applied it to the lamellar phase. These methods are based on the observation that, if one compares the electron densities of two lamellar phases with slightly different water contents, the correct phasing should yield the electron density that changes the least in going from one hydration to another. This is known as the swelling method of phasing.

Quantitatively, one can define the difference in electron densities as

$$\Delta = \frac{1}{A} \int (\rho_e'(\mathbf{r} + \delta) - C\rho_e(\mathbf{r}) - B)^2 \, dA, \qquad (4)$$

where Δ is a measure of the deviation, A is the area of the unit cell, ρ_e' is the electron density at one hydration, ρ_e is the electron density at another hydration, δ is the small difference in the radii of the two water cores, and B and C are constants to take into account differences in absolute and relative scaling, and the integral is performed over the unit cell (Turner and Gruner, 1992). Minimizing Δ with respect to B and C yields the following formulas for those quantities:

$$C = \frac{A\int \rho_e'(\mathbf{r} + \delta)\rho_e(\mathbf{r}) \, dA - \int \rho_e'(\mathbf{r} + \delta) dA \int \rho_e(\mathbf{r}) \, dA}{A\int (\rho_e(\mathbf{r}))^2 \, dA - (\int \rho_e(\mathbf{r}) \, dA)^2},$$
$$(5)$$

$$B = \frac{1}{A}\left[\int \rho_e'(\mathbf{r} + \delta) \, dA - C \int \rho_e(\mathbf{r}) \, dA \right]. \qquad (6)$$

For the H_{II} phase, the electron density is given by

$$\rho_{hex}(x, y) = \rho_{avg} + \sum_{h=1}^{\infty} \sum_{k=1}^{\infty} A_{hk}[\cos(hA + kB) + \cos(hA$$
$$- (h + k)B) + \cos((h + k)A - kB)]$$
$$+ \sum_{h=0}^{\infty} \sum_{k=0}^{\infty} A_{hk}^{(h \neq 0 \text{ and } k=0) \text{ or } (h=0 \text{ and } k \neq 0)}[\cos(hA$$
$$+ kB) + \cos(h + k)(A - B))/2], \quad (7)$$

where

$$A = \frac{2\pi(x - y \cot(\pi/3))}{d}, \qquad (8)$$

$$B = \frac{2\pi y}{d \sin(\pi/3)}. \qquad (9)$$

For h or k equal to 0 or $h = k$, the multiplicity for the A_{hk} is 6. For the remaining cases, the multiplicity is 12.

X-ray diffraction

X-ray diffraction data were acquired as described in Lewis et al. (1989) but with the intensifier/lens/CCD detector described in Tate et al. (1997). Briefly, x-rays were generated on a Rigaku RU-200 rotating anode x-ray generator using a copper anode. The beam was Ni-filtered, point focused via two orthogonal Franks mirrors and the data were recorded on a two-dimensional x-ray detector based on an intensified CCD. Samples consisted of unoriented dispersions of fully hydrated lipid and water, generally in an ~1:1 weight ratio, contained in 1.5 mm glass x-ray capillaries. The x-ray stage was thermostatically controlled to ~0.5°C and a stability of ~0.1°C. Equilibration of the samples was checked by varying the equilibration time between temperature steps until the diffraction was stable when the time was increased. Repeat spacings were calibrated with silver stearate, which has a lamellar repeat of 48.68 Å (Vand et al., 1949).

RESULTS

Lamellar reconstructions

Diffraction is seen to fourth order for lipids in the L_α phase. The Lorentz-corrected amplitudes as a function of temperature are listed for each lipid in Table 3. Note that the amplitudes have been normalized to the first-order amplitude and that the multiplicity for each of these peaks is the same.

Four diffracted orders can have $2^4 = 16$ possible combinations of sign; however, eight of these are simply the negative of the remaining eight combinations (cf. Figs. 2 and 3). Choosing a phasing that is centered on the midplane of the bilayer requires that the middle of the electron density profile be coincident with the terminal methyl dip, thereby eliminating 8 of the 16 possible phase combinations. The remaining combinations are shown in Fig. 2. The minimum must also be bounded by maxima due to the phospholipid headgroups, followed by a decrease in electron density in the water region. The average electron density is set to zero, as noted earlier, and because the electron density of water is about equal to the average electron density of the system, one expects a substantial decrease in the electron density toward zero in the water region. This leaves only $--+-$ and $-++-$ as viable choices, with a preference toward $--+-$, because the dip in the water region is slightly deeper. To resolve this choice satisfactorily, note that it has been shown that 18:1$c\Delta$9-PE has a phasing of $--+-$ (So et al., 1993). Because 18:1$c\Delta$9-PE is practically identical to 18:1$t\Delta$9-PE in terms of electron density, it seems clear that this is the proper phasing for 18:1$t\Delta$9-PE as well.

For the other lipids studied besides 18:1$c\Delta$9-PE and 18:1$t\Delta$9-PE (except for 21:0$_{ch}$-PE), the weak second-order reflection was missing, and so it was straightforward to pick the correct phasing, which was $-0+-$. The correct phasing for 21:0$_{ch}$-PE was $-++-$, as shown by the following reasoning. The strong first-order peak must have a minus phasing for the hydrocarbon region to have a lower electron density than the headgroups and the water. A plot of the remaining phase combinations is shown in Fig. 4. The 21:0$_{ch}$-PE has no terminal methyls and must therefore have a relatively uniform electron density in the hydrocarbon region. The only phase combination that satisfies this is $-++-$. It is not surprising that most of these lipids have the same phasing because the overall chemical structure of all these lipids is quite similar. Finally, note that these phase choices yield water-layer thicknesses that are the same to within an angstrom for all of the lipids. Because it is reasonable that lipids with the same headgroup and similar hydrocarbon chains should have the same water-layer spacing, this helps confirm these phasing choices.

Inverted hexagonal reconstructions

This method was applied to 18:1$c\Delta$9-PE using the amplitudes at 85°C and 95°C. The amplitudes for 18:1$c\Delta$9-PE in

TABLE 3 Temperature (*T*, °C), measured amplitudes, *d*, *w*, ⟨*l*⟩, *v*, and *A* for several hydrocarbon chain structural variants of diacyl phosphatidylethanolamine in the L$_\alpha$ phase

	Lamellar Phase Data								
	Amplitudes				*d*	*w*	⟨*l*⟩	*v*	*A*
T (°C)	1	2	3	4	(Å)	(Å)	(Å)	(Å³)	(Å²)
18:1*c*Δ9-PE									
−4	1.0	0.09	0.20	0.30	53.1	13.1	20.1	1190	59.3
0	1.0	0.10	0.20	0.30	52.9	13.0	20.0	1190	59.7
4	1.0	0.09	0.21	0.29	52.6	13.0	19.9	1190	60.3
20:0$_{eai}$-PE									
30	1.0	0.0	0.16	0.33	58.9	13.8	22.6	1340	59.4
35	1.0	0.0	0.16	0.33	58.2	13.6	22.3	1340	60.3
40	1.0	0.0	0.16	0.33	57.6	13.5	22.1	1350	61.1
45	1.0	0.0	0.15	0.31	57.1	13.2	22.0	1350	61.6
50	1.0	0.0	0.16	0.31	56.6	13.2	21.8	1360	62.6
18:1*t*Δ9-PE									
50	1.0	0.08	0.20	0.27	53.3	13.0	20.2	1210	60.4
55	1.0	0.08	0.19	0.26	52.7	12.9	20.0	1220	61.2
60	1.0	0.08	0.19	0.26	52.2	12.7	19.8	1220	62.0
20:0$_{dmi}$-PE									
40	1.0	0.0	0.11	0.33	60.0	13.7	23.2	1370	59.0
45	1.0	0.0	0.12	0.33	59.3	13.6	22.9	1370	59.9
50	1.0	0.0	0.11	0.32	58.7	13.3	22.7	1380	60.7
55	1.0	0.0	0.10	0.32	58.1	13.1	22.5	1380	61.4
60	1.0	0.0	0.09	0.32	57.5	12.9	22.3	1390	62.2
65	1.0	0.0	0.09	0.31	57.0	12.7	22.2	1390	62.9
70	1.0	0.0	0.08	0.29	56.5	12.5	22.0	1400	63.5
19:0$_{ai}$-PE									
50	1.0	0.0	0.14	0.34	57.9	13.4	22.3	1310	59.1
55	1.0	0.0	0.13	0.34	57.2	13.2	22.0	1320	59.9
60	1.0	0.0	0.14	0.32	56.5	13.0	21.8	1320	60.9
65	1.0	0.0	0.13	0.32	55.9	12.9	21.6	1330	61.7
70	1.0	0.0	0.13	0.30	55.3	12.6	21.4	1330	62.5
75	1.0	0.0	0.12	0.30	54.8	12.5	21.2	1340	63.2
80	1.0	0.0	0.12	0.28	54.2	12.3	21.0	1340	64.0
21:0$_{ch}$-PE									
55	1.0	0.16	0.24	0.38	60.4	13.9	23.3	1370	58.7
60	1.0	0.15	0.21	0.38	59.5	13.5	23.0	1370	59.6
65	1.0	0.17	0.22	0.36	58.8	13.3	22.8	1370	60.5
70	1.0	0.16	0.21	0.35	58.0	13.1	22.5	1380	61.5
75	1.0	0.16	0.20	0.35	57.4	12.9	22.3	1380	62.3
80	1.0	0.16	0.19	0.33	56.8	12.6	22.2	1390	62.9
19:0$_i$-PE									
66	1.0	0.0	0.10	0.34	57.4	13.0	22.3	1330	60.1
70	1.0	0.0	0.09	0.31	56.8	12.7	22.1	1340	60.7
74	1.0	0.0	0.11	0.31	56.2	12.7	21.8	1340	61.8
78	1.0	0.0	0.10	0.29	55.7	12.5	21.6	1350	62.3
82	1.0	0.0	0.10	0.29	55.2	12.3	21.5	1350	63.0
86	1.0	0.0	0.11	0.29	54.7	12.3	21.3	1350	63.9

The amplitudes have been Lorentz- and multiplicity-corrected and have been normalized to the first-order amplitude (see text).

d, d-spacing; *w*, water-layer thickness; *l*, lipid length; *v*, lipid volume; and *A*, headgroup area at the lipid–water interface. The estimated accuracies are ±0.5 Å for *d* and *w*, ±0.25 Å for ⟨*l*⟩, ±20 Å³ for *v*, and ±1.5 Å² for *A*.

the H$_{II}$ phase are shown in Table 4 and the amplitudes for the other lipids in the H$_{II}$ phase are shown in Table 5. According to the phasing criteria developed by Turner and Gruner (1992), the best phasing is selected by first eliminating from consideration all phase sets with a scale factor

C that varies from 1 by more than 0.05 and then picking the phasing with the lowest Δ from the remaining choices. The best phasing choice was (+ − − + + + +) according to the above criteria, with the second-best phase choice having a value of Δ that was twice as large. This is also the phasing found for the H$_{II}$ phases of 18:1*c*Δ9-PE by Turner and Gruner (1992). A reconstruction of 18:1*t*Δ9-PE using the + − − + + + + phasing is shown in a 3D plot in Fig. 5. The electron density shown is similar to that of 18:1*c*Δ9-PE (Turner and Gruner, 1992).

The phasing + − − + + + + was also found to be the correct phasing for the other PEs studied, using the same phasing method. This is a reasonable result, considering the similarity of the lipids. As will be shown in the following section, several patterns emerge in the structural parameters that also help confirm this phasing choice. For example, the average lipid length appears to decrease by roughly the same amount (1–1.5 Å) across the L$_\alpha$/H$_{II}$ phase transition for all the lipids studied. Additionally, the headgroup areas at the lipid–water interface assume similar values. This physically plausible behavior lends support to the phasing choice.

Structural parameters

The structural parameters of the L$_\alpha$ and H$_{II}$ phases are defined in Fig. 6. The dimensions that were found, as described below, are listed in Tables 4–6 and Figs. 6–10. The value of *d* is readily measured to an accuracy of ±½ Å and the position of the lipid–water interface can also be calculated from the electron density reconstruction to a relative accuracy of ±½ Å (Turner and Gruner, 1992). Though disorder is certainly present in these systems, the method used to determine the lipid–water interface uses experimental amplitudes that have not been altered to correct for disorder. The values of *d* are given in Fig. 7, and the values of the water layer thickness (*w* and *r*, as defined in Fig. 6) are given in Fig. 8.

The d-spacings for the L$_\alpha$ and H$_{II}$ phases formed by the various PEs are presented in Fig. 7. In both phases, they decrease as a function of increasing temperature, although, in general, the rate of decrease is smaller in the L$_\alpha$ phase than in the H$_{II}$ phase. The rate of decrease of the d-spacings with temperature in both phases does not depend significantly on chain structure. However, as shown in Table 6, the magnitudes of the d-spacings of the L$_\alpha$ and H$_{II}$ phases at temperatures either side of their L$_\alpha$/H$_{II}$ phase transitions do depend significantly on the structure of the hydrocarbon chains. In particular, the d-spacings in the L$_\alpha$ phase varied from 51.2 to 56.4 Å and those in the H$_{II}$ phase from 74.9 to 82.7 Å. These results differ from those reported in our earlier study (Lewis et al., 1989), where near-constant d-spacings of 52.5 and 77.0–78.0 Å for the L$_\alpha$ and H$_{II}$ phases, respectively, were reported for these PEs. Interestingly, the values of the d-spacings for the 18:1*c*Δ9- and 18:1*t*Δ9-PEs
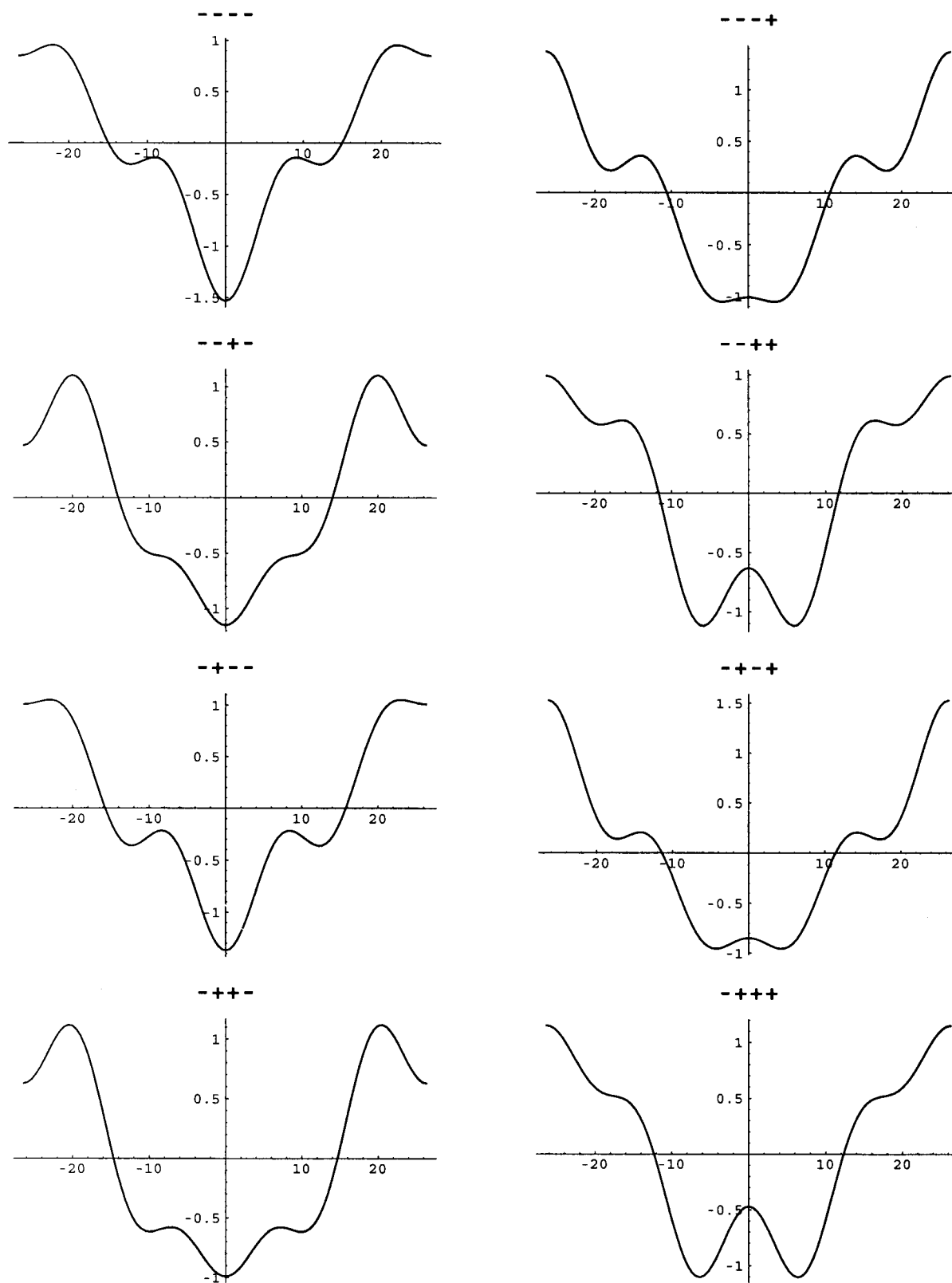
FIGURE 2 Electron density reconstructions of the L_α phase for 18:1tΔ9-PE at 55°C. The phasing is shown above the reconstruction. Only phasing combinations in which the first phase is negative are shown in this figure. The y-axis is the electron density in arbitrary units and the x-axis is in angstroms.
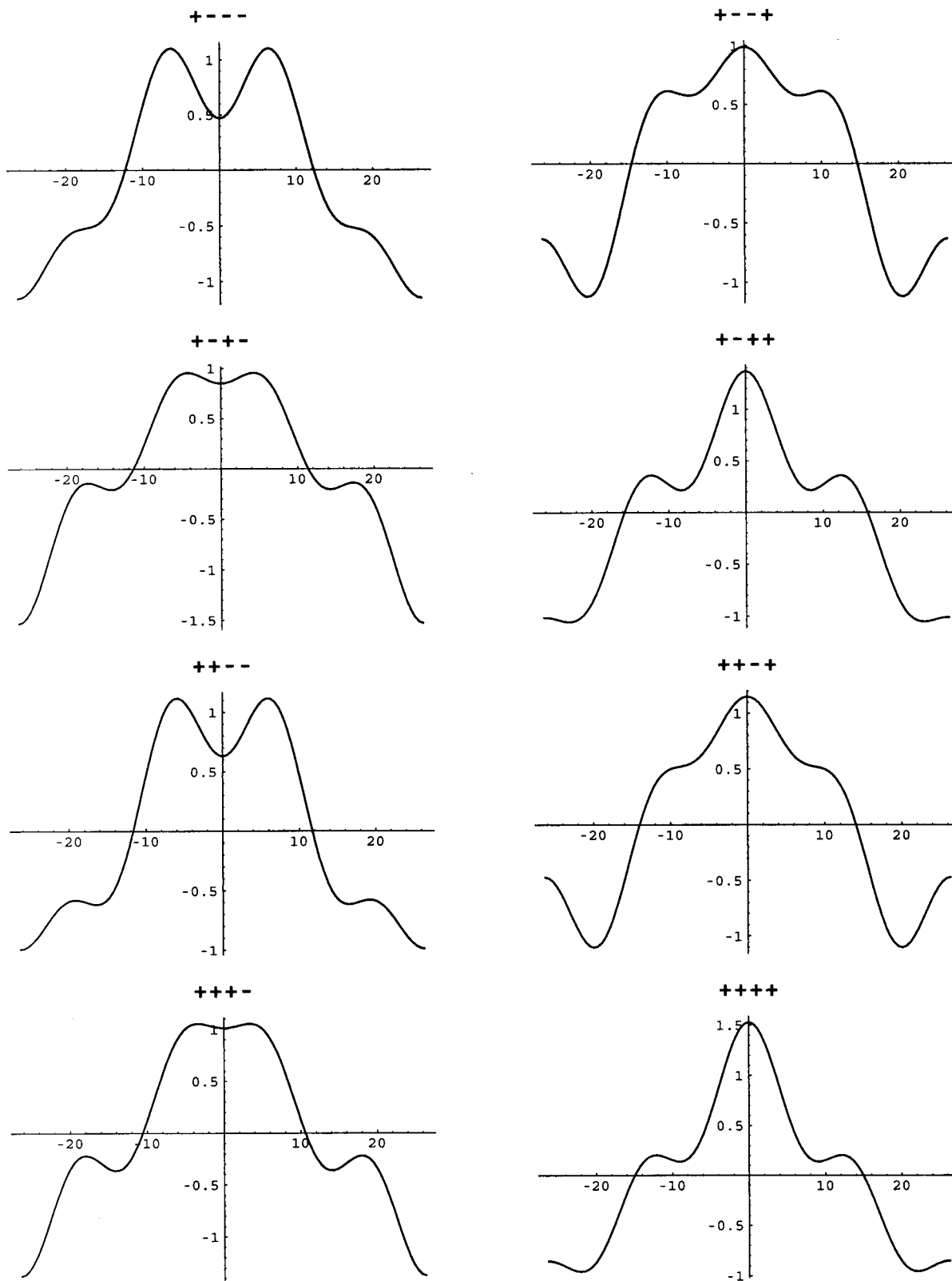
FIGURE 3   Electron density reconstructions of the L$_\alpha$ phase for 18:1$t\Delta$9-PE at 55°C. The phasing is shown above the reconstruction. Only phasing combinations in which the first phase is positive are shown in this figure. The y-axis is the electron density in arbitrary units and the x-axis is in angstroms.
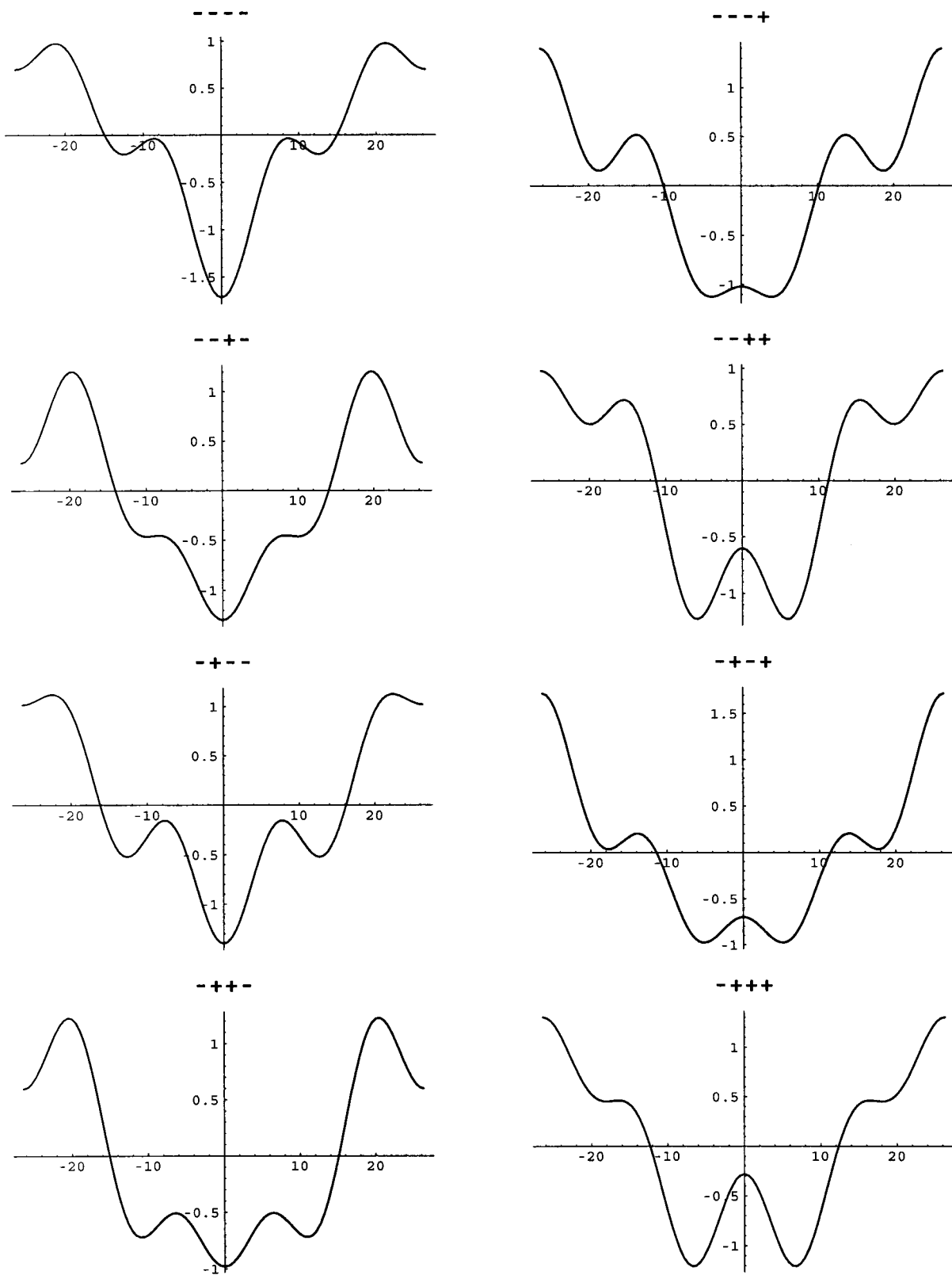
FIGURE 4 Electron density reconstructions of the L_α phase for $21{:}0_{ch}$-PE at 70°C. The phasing is shown above the reconstruction. The y-axis is the electron density in arbitrary units and the x-axis is in angstroms.

TABLE 4 Temperature (*T*, °C), measured amplitudes, *d*, *r*, $\langle l \rangle$, *v*, and *A* for 1,2-di-O-oleoyl-3-O-phosphatidylethanolamine-*sn*-glycerol in the H$_{II}$ phase

	18:1$c\Delta$9-PE Hexagonal Phase Data														
	Amplitudes										d	r	$\langle l \rangle$	v	A
T (°C)	1, 0	1, 1	2, 0	2, 1	3, 0	2, 2	3, 1	4, 0	3, 2	4, 1	(Å)	(Å)	(Å)	(Å^3)	(Å^2)
4	1.0	1.19	0.95	0.33	0.30	0.20	0.14	0	0.14	0.15	79.8	23.8	18.3	1190	47.8
8	1.0	1.13	0.91	0.29	0.29	0.18	0.14	0	0.13	0.12	78.5	23.2	18.2	1200	47.8
12	1.0	1.11	0.89	0.27	0.27	0.20	0.15	0	0.11	0.14	77.3	22.6	18.2	1200	47.8
20	1.0	1.04	0.83	0.21	0.24	0.18	0.15	0	0.09	0.11	75.3	21.6	18.1	1210	47.6
30	1.0	0.96	0.78	0.16	0.21	0.18	0.14	0	0.00	0.00	72.9	20.4	18.0	1220	47.4
40	1.0	0.90	0.75	0.13	0.17	0.21	0.16	0	0.00	0.00	70.8	19.4	17.9	1230	47.2
50	1.0	0.85	0.72	0.09	0.15	0.18	0.15	0	0.00	0.00	68.9	18.5	17.8	1230	47.2
60	1.0	0.80	0.68	0.06	0.12	0.16	0.14	0	0.00	0.00	67.2	17.9	17.5	1240	47.8
70	1.0	0.75	0.65	0.0	0.12	0.14	0.13	0	0.00	0.00	65.7	17.2	17.4	1250	48.3
80	1.0	0.71	0.62	0.0	0.09	0.14	0.12	0	0.00	0.00	64.2	16.7	17.1	1260	48.8
90	1.0	0.69	0.60	0.0	0.09	0.14	0.12	0	0.00	0.00	62.9	16.2	17.0	1270	49.8

The amplitudes have been Lorentz- and multiplicity-corrected and have been normalized to the first-order amplitude (see text). *d*, d-spacing; *r*, average water radius; $\langle l \rangle$, average lipid length; *v*, lipid volume; and *A*, headgroup area at the lipid–water interface.
The estimated accuracies are ±0.5 Å for *d*, *r*, and $\langle l \rangle$, ±20 Å^3 for *v*, and ±2 Å^2 for *A*.

are the smallest in both the L$_\alpha$ and H$_{II}$ phases, whereas those for 19:0$_i$ and 19:0$_{ai}$-PE are intermediate, and those for the 20:0$_{eai}$, 20:0$_{dmi}$ and 21:0$_{ch}$-PE are largest. The possible molecular basis for these observations will be discussed in a forthcoming paper to be presented elsewhere (D. A. Mannock, R. N. A. H. Lewis, R. N. McElhaney, P. E. Harper, and S. M. Gruner, submitted for publication).

The dependence of the water-layer dimensions for the L$_\alpha$ and H$_{II}$ phases formed by the various PEs studied here as a function of temperature are presented in Fig. 8. In general, the thickness of the water layer separating adjoining bilayers in the L$_\alpha$ phase is much less than the radius of the central water core in the H$_{II}$ phase, as expected. The L$_\alpha$ phase water-layer thickness (12.2–13.1 Å) also varies less with changes in the structure of the hydrocarbon chains than does the radius of the water core in the H$_{II}$ phase, which varies from 20.9 to 23.1 Å (Table 6). Nevertheless, these values vary much less with PE hydrocarbon chain structure than do the d-spacings, indicating that variations in average lipid length and headgroup area at the lipid–water interface must account for most of the observed variations in the bilayer d-spacing. However, the small variations in the radius of the water cylinders in the H$_{II}$ phase formed by the various PEs follow the same trends as those observed in the d-spacings of the L$_\alpha$ and H$_{II}$ phases, suggesting that the structure of the chains also plays a part in determining the monolayer curvature in the H$_{II}$ phase. With the lipid volumes, *V*, discussed in the Methods section and a coefficient of expansion of $\Delta V/V \simeq 7 \times 10^{-4}$/°C, one can use geometry to calculate the headgroup area at the lipid–water interface. For the L$_\alpha$ case, the headgroup area is given by

$$A = V/l, \tag{10}$$

and, for the H$_{II}$ case,

$$A = V\left(\frac{2\pi r}{(\sqrt{3}/2)d^2 - \pi r^2}\right), \tag{11}$$

where *A* is headgroup area at the lipid–water interface, *V* is the lipid volume, *d* is d-spacing, and *r* is the water core radius, all of which are defined in Fig. 6. As expected, the headgroup areas at the lipid–water interface (Fig. 9) are considerably larger and increase more rapidly with increases in temperature in the L$_\alpha$ phase than in the H$_{II}$ phase. However, the most important feature of this plot, and the data in Table 6, is that the headgroup areas at the lipid–water interface in both the L$_\alpha$ and H$_{II}$ phases just below and just above the L$_\alpha$/H$_{II}$ phase transition are quite similar for each PE hydrocarbon chain variant. These results suggest that the effects emanating from the variation in the structure of hydrocarbon chains on the headgroup area at the lipid–water interface are relatively small.

The average lipid lengths are shown in Fig. 10. In calculating the average lipid length for the H$_{II}$ phase, each length was weighted by the volume of lipid for that length. If one assumes that the volume of each lipid in a given phase at a given temperature is constant, then weighting averages by volume is equivalent to averaging over all the lipids. The derivation for the formula for the average length in the H$_{II}$ phase is as follows. From Fig. 6, it is noted that $l(\theta)$, the lipid length as a function of θ (in radians), is defined

$$l(\theta = 0) = l_{min}, \tag{12}$$

$$l\left(\theta = \frac{\pi}{6}\right) = l_{max}. \tag{13}$$

From geometry,

$$(r + l)\cos \theta = r + l_{min}, \tag{14}$$

TABLE 5 Temperature (*T*, °C), measured amplitudes, *d*, *r*, ⟨*l*⟩, *v* and *A* for several hydrocarbon chain structural variants of diacyl phosphatidylethanolamine in the H$_{II}$ phase

	Hexagonal Phase Data											
	Amplitudes							*d*	*r*	⟨*l*⟩	*v*	*A*
T (°C)	1, 0	1, 1	2, 0	2, 1	3, 0	2, 2	3, 1	(Å)	(Å)	(Å)	(Å³)	(Å²)
20:0$_{eai}$-PE												
65	1.0	0.86	0.75	0.11	0.19	0.22	0.15	80.7	21.9	20.6	1370	45.7
70	1.0	0.82	0.71	0.07	0.20	0.20	0.17	78.7	21.2	20.3	1380	46.4
75	1.0	0.79	0.69	0.00	0.14	0.20	0.16	77.0	20.3	20.3	1380	45.8
80	1.0	0.76	0.68	0.00	0.14	0.16	0.16	75.4	19.8	19.9	1390	46.5
85	1.0	0.73	0.66	0.00	0.13	0.17	0.15	74.0	19.3	19.7	1390	47.4
90	1.0	0.71	0.63	0.00	0.10	0.16	0.15	72.7	18.9	19.4	1400	47.8
95	1.0	0.68	0.62	0.00	0.11	0.18	0.14	71.4	18.5	19.1	1400	48.9
18:1*t*Δ9-PE												
65	1.0	0.99	0.79	0.20	0.23	0.18	0.13	75.2	21.0	18.7	1230	46.0
70	1.0	0.96	0.77	0.16	0.21	0.17	0.14	73.7	20.4	18.5	1230	46.2
75	1.0	0.92	0.76	0.14	0.20	0.16	0.14	72.4	19.9	18.3	1240	46.7
80	1.0	0.90	0.74	0.11	0.19	0.17	0.14	71.1	19.4	18.1	1240	47.0
85	1.0	0.88	0.73	0.10	0.17	0.18	0.14	69.9	18.9	17.9	1250	47.6
90	1.0	0.85	0.70	0.07	0.16	0.17	0.13	68.8	18.4	17.9	1250	47.7
95	1.0	0.84	0.71	0.00	0.15	0.18	0.14	67.7	17.8	17.9	1250	47.3
20:0$_{dmi}$-PE												
75	1.0	0.87	0.73	0.15	0.19	0.18	0.15	82.6	22.6	21.0	1400	46.4
80	1.0	0.83	0.70	0.11	0.16	0.18	0.16	80.3	21.7	20.6	1410	46.7
85	1.0	0.80	0.69	0.07	0.17	0.19	0.15	78.3	21.0	20.3	1410	47.3
90	1.0	0.76	0.66	0.00	0.14	0.17	0.16	76.5	20.1	20.2	1420	46.8
95	1.0	0.74	0.64	0.00	0.15	0.18	0.15	74.9	19.6	19.9	1420	48.0
19:0$_{ai}$-PE												
85	1.0	0.89	0.74	0.10	0.19	0.20	0.15	77.2	21.0	19.7	1350	46.8
90	1.0	0.85	0.72	0.08	0.17	0.19	0.15	75.5	20.3	19.5	1350	47.4
95	1.0	0.83	0.70	0.06	0.15	0.19	0.15	73.9	19.7	19.3	1360	48.0
21:0$_{ch}$-PE												
85	1.0	0.92	0.84	0.00	0.25	0.28	0.22	79.6	21.4	20.6	1390	46.1
90	1.0	0.87	0.80	0.00	0.23	0.28	0.20	77.4	20.7	20.1	1400	47.4
95	1.0	0.82	0.78	0.00	0.16	0.26	0.22	75.4	20.0	19.8	1400	48.0
19:0$_i$-PE												
90	1.0	0.86	0.71	0.12	0.21	0.21	0.13	78.4	21.4	19.9	1360	47.0
94	1.0	0.84	0.70	0.09	0.20	0.20	0.13	76.8	20.8	19.7	1360	47.4
98	1.0	0.82	0.69	0.08	0.16	0.20	0.12	75.4	20.3	19.5	1360	47.8

The amplitudes have been Lorentz- and multiplicity-corrected and have been normalized to the first-order amplitude (see text).
d, d-spacing; *r*, average water radius; ⟨*l*⟩, average lipid length; *v*, is the lipid volume; and *A*, is the headgroup area at the lipid–water interface.
The estimated accuracies are ±0.5 Å for *d*, *r*, and ⟨*l*⟩, ±20 Å³ for *v*, and ±2 Å² for *A*.

where r is the water core radius, l is lipid length as a function of θ, and l_{min} is minimum value of $l(\theta)$, as shown in Fig. 6. Define

$$\beta \equiv \frac{r}{l_{min}} \quad (15)$$

for computational convenience. Solving for l yields

$$l = (r + l_{min})\sec\theta - r \quad (16)$$

$$= l_{min}[(\beta + 1)\sec\theta - \beta^2]. \quad (17)$$

For the area S, as in Fig. 6,

$$\frac{dS}{d\theta} = \frac{\pi(r + l)^2 - \pi r^2}{2\pi} \quad (18)$$

$$= \tfrac{1}{2}[(r + l_{min})^2\sec^2\theta - r^2] \quad (19)$$

$$= \tfrac{1}{2}l_{min}[(\beta + 1)^2\sec^2\theta - \beta^2]. \quad (20)$$

Finally, ⟨*l*⟩, the average lipid length, is given by

$$\langle l \rangle \equiv \int l\, dV \Big/ \int dV \quad (21)$$

$$= \int_0^{\pi/6} l\, \frac{dS}{d\theta}\, d\theta \Big/ \int_0^{\pi/6} \frac{dS}{d\theta}\, d\theta, \quad (22)$$

which to first order in $(\beta - 1)$, is
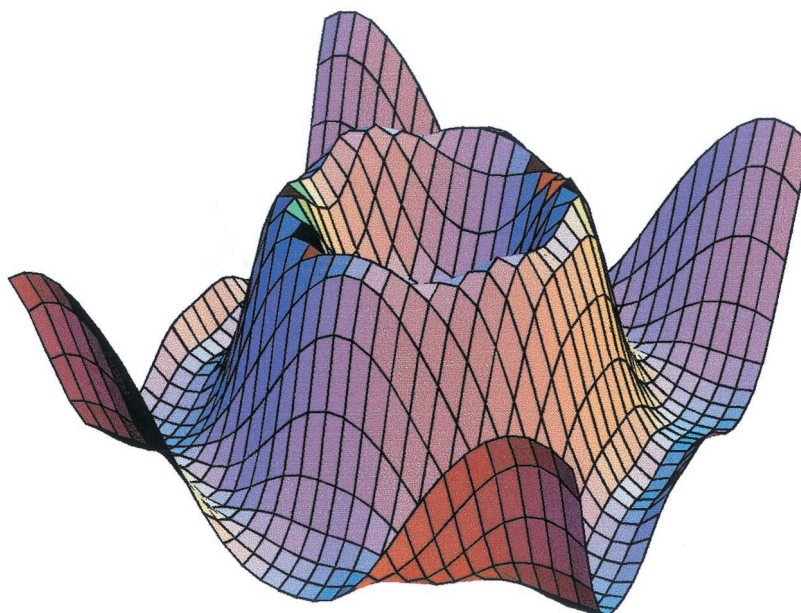
$$\cong l_{min}[1.1084 + 0.0572(\beta - 1)]. \quad (23)$$

FIGURE 5   A 3D view of the electron density reconstruction of the H_{II} phase for 18:1$t\Delta$9-PE at 85°C.

Note that the expansion for $\langle l \rangle$ is accurate to $\pm 0.2\%$ for $0.5 < \beta < 1.5$.

The dependence of lipid length on temperature in the L_α and H_{II} phases formed by the various PEs studied here is presented in Fig. 10. In all cases, the lipid lengths decrease with increasing temperature in both phases at roughly comparable rates with an abrupt decrease of 1.5–2.0 Å at the L_α/H_{II} phase transition, as expected (Table 6). The magnitude of the lipid length values also changes with hydrocarbon chain structure as was observed with the d-spacings. Typically, the lipid lengths in both the L_α and H_{II} phases of the 18:1$c\Delta$9- and 18:1$t\Delta$9-PEs are smallest, those for 19:0$_i$ and 19:0$_{ai}$-PE are intermediate, and those for the 20:0$_{eai}$, 20:0$_{dmi}$, and 21:0$_{ch}$-PE are the largest. Thus, the bulk and position of the substituent branch on the hydrocarbon chain determine T_h by moderating the ability of the hydrocarbon chains to shorten as a function of increasing temperature. Once again, the possible molecular basis for these observations will be discussed in a forthcoming paper to be presented elsewhere (D. A. Mannock, R. N. A. H. Lewis, R. N. McElhaney, P. E. Harper, and S. M. Gruner, submitted for publication).

DISCUSSION

The original impetus for this study came from an observation that, at the L_α/H_{II} phase transition, all of these PEs had very similar L_α and H_{II} d-spacings (Lewis et al., 1989). The goal of this study was to check whether the internal dimensions followed the same pattern. In fact, it turns out that the dimensions, both internal and external, vary by over 10%. The difference with our earlier measurements (Lewis et al.,
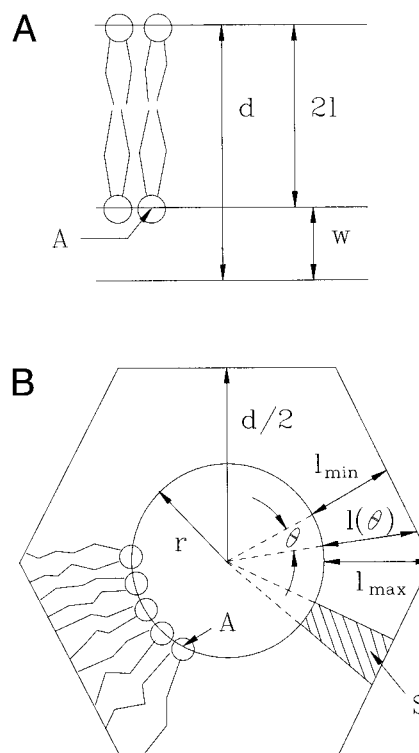

FIGURE 6   Typical terminology used in this study. (A) The L_α dimensions, d is the d-spacing, l is the lipid length, and w is the thickness of the water layer between the lipid bilayers. (B) The H_{II} dimensions, d is the d-spacing, l_{min} is the minimum lipid length, l_{max} is the maximum lipid length, and r is the water core radius. Note that in both diagrams, A is the headgroup area at the lipid–water interface and S is the area of the hatched region.
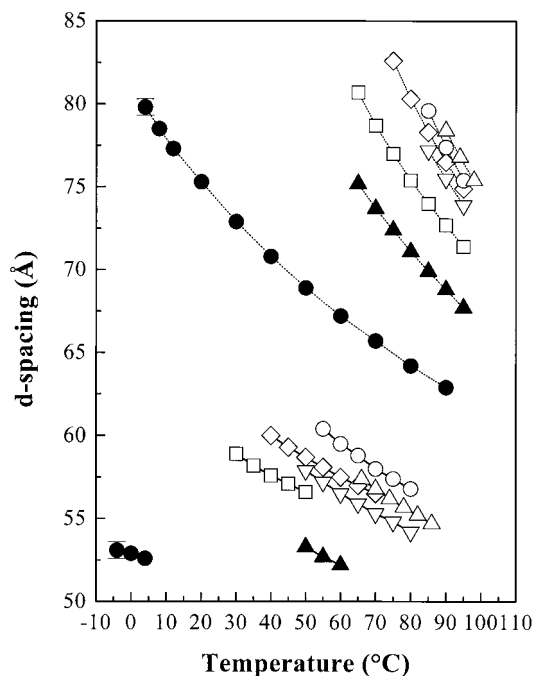
FIGURE 7 Unit cell lengths (*d* in Fig. 6) for some hydrocarbon chain structural variants of diacyl phosphatidylethanolamine. Solid lines connect the L_α data points and dotted lines connect the H_{II} data points. Representative error bars for each phase are plotted for 18:1$c\Delta$9-PE at one data point per phase. ●, 18:1$c\Delta$9-PE; ▲, 18:1$t\Delta$9-PE; □, 20:0$_{eai}$-PE; ◇, 20:0$_{dmi}$-PE; △, 19:0$_i$-PE; ▽, 19:0$_{ai}$-PE; ○, 21:0$_{ch}$-PE.

1989) has been traced to faulty temperature calibration. This result underscores the need for accurate temperature calibrations.

Besides correcting the earlier study, there are a number of interesting features of the data that add insight into PE phase behavior. The first is that the water–layer thickness in the L_α phase is the same to within one angstrom for all of these PEs (Fig. 8). This suggests that the headgroup plays the dominant role in setting the interlamellar water-layer thickness, with the hydrocarbon chains playing a secondary role. It is also interesting to note that the water layer shrinks at roughly the same rate as the increase of the headgroup area at the lipid–water interface, implying that the property of the headgroups that sets the water-layer spacing varies inversely with the headgroup area.

The rate of contraction of the hydrocarbon chains with increasing temperature for a given lipid is roughly the same in both the L_α and H_{II} phases. There is also a small decrease in $\langle l \rangle$ of ~1.0–2.0 Å across the phase transition, an amount that is approximately the same for all the PEs under study (Fig. 10). The behavior of the headgroup area at the lipid–water interface is far more dramatic, as the headgroup area increases in the L_α phase, and then drops dramatically across the L_α/H_{II} phase transition. The headgroup areas at
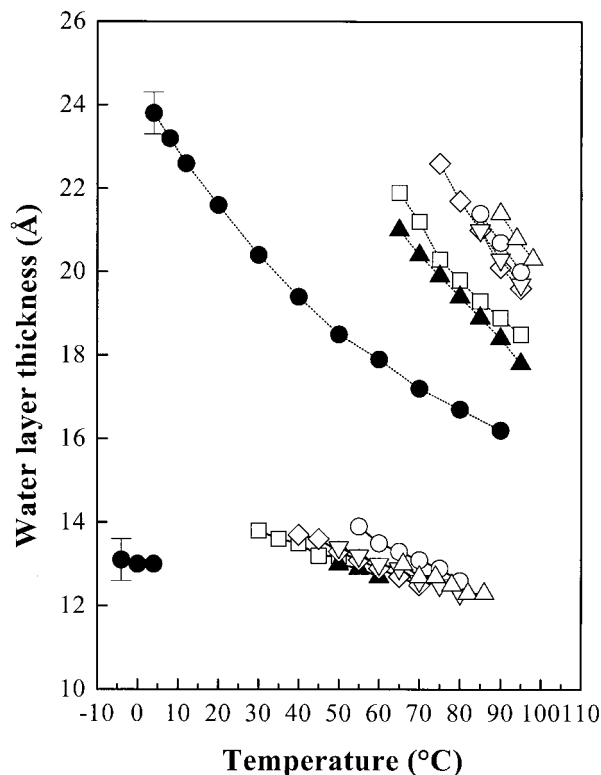
FIGURE 8 Water layer thickness (*w* or *r* in Fig. 6) for some hydrocarbon chain structural variants of diacyl phosphatidylethanolamine. Solid lines connect the L_α data points and dotted lines connect the H_{II} data points. Representative error bars for each phase are plotted for 18:1$c\Delta$9-PE at one data point per phase. The symbols have the same meaning as in Fig. 7.

the lipid–water interface also tend to have similar values in the H_{II} phase (Fig. 9) regardless of the hydrocarbon chain structure.

TABLE 6 Lipid dimensions (d-spacing, *w*, *r*, $\langle l \rangle$ and *A*) at the L_α/H_{II} phase transition for the hydrocarbon chain structural variants of diacyl phosphatidylethanolamine used in this study

Diacyl-PE	ECL = 18 Carbons		Additional PE Structural Parameters					
	d-spacing		L_α phase			H_{II} phase		
Chain Structure	$T_{L/NL}$ (°C)	L_α (Å)	H_{II} (Å)	*w* (Å)	$\langle l \rangle$ (Å)	*A* (Å)	*r* (Å)	$\langle l \rangle$ (Å)	*A* (Å)
18:1$c\Delta$9-PE	10.0	52.1	77.9	12.8	19.7	61.0	22.9	17.6	47.7
18:1$t\Delta$9-PE	65.0	51.6	75.0	12.5	19.5	62.8	20.9	18.2	46.1
20:0$_{eai}$-PE	52.0	56.3	84.2	13.1	21.6	62.8	23.1	20.9	44.1
20:0$_{dmi}$-PE	74.0	55.9	82.7	12.3	21.8	64.2	22.7	20.5	46.2
19:0$_{ai}$-PE	80.5	54.0	78.6	12.2	20.9	64.1	21.5	19.6	46.3
19:0$_i$-PE	88.0	54.4	79.1	12.2	21.1	64.2	21.7	19.7	46.7
21:0$_{ch}$-PE	82.8	56.3	80.5	12.4	21.9	63.5	21.6	20.5	45.7

Dimensions at the L_α/H_{II} phase transition were determined by making a linear fit of the experimental data as function of temperature for each phase and then extrapolating the line to the phase transition temperature as determined by the DSC. In the case of 18:1$c\Delta$9-PE in the hexagonal phase, quadratic curve fitting procedure was used.
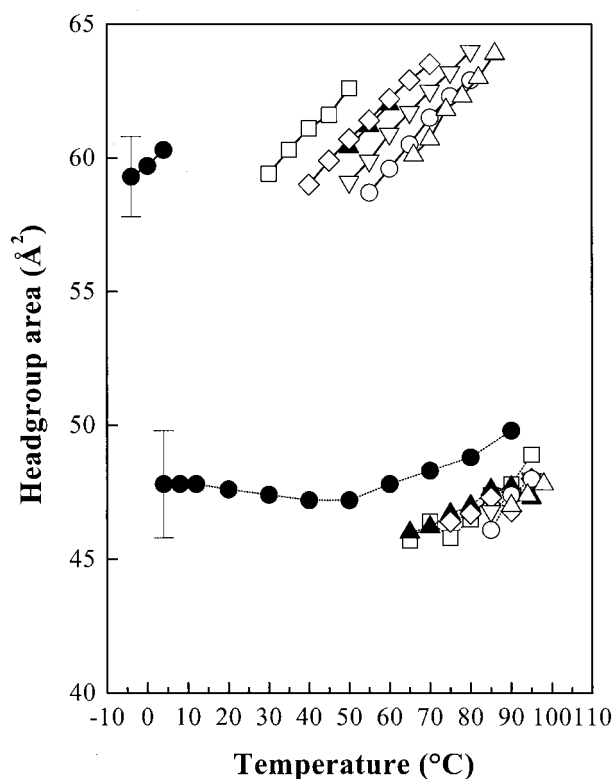
FIGURE 9 Headgroup area at lipid–water interface (A in Fig. 6) for some hydrocarbon chain structural variants of diacyl phosphatidylethanolamine. Solid lines connect the L$_\alpha$ data points and dotted lines connect the H$_{II}$ data points. Representative error bars for each phase are plotted for 18:1cΔ9-PE at one data point per phase. The symbols have the same meaning as in Fig. 7.
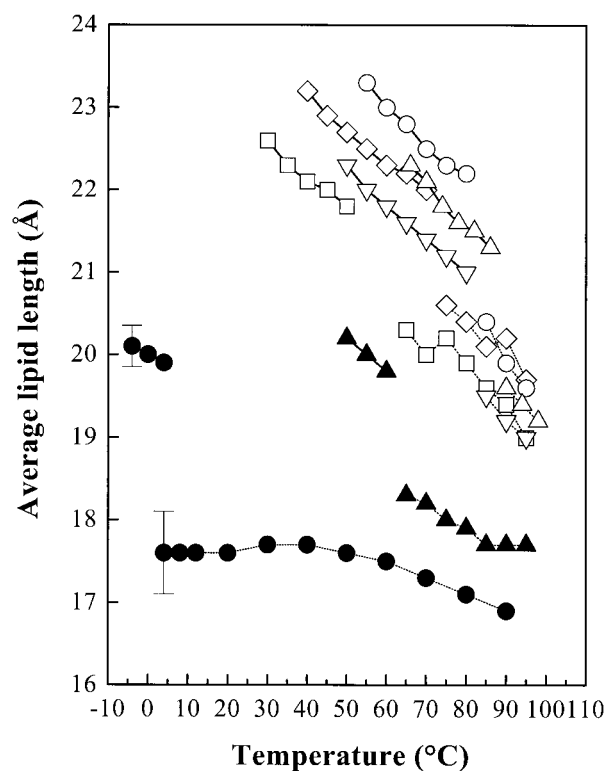
FIGURE 10 Average lipid length ($\langle l \rangle$ in Fig. 6) for some hydrocarbon chain structural variants of diacyl phosphatidylethanolamine. Solid lines connect the L$_\alpha$ data points and dotted lines connect the H$_{II}$ data points. Representative error bars for each phase are plotted for 18:1cΔ9-PE at one data point per phase. The symbols have the same meaning as in Fig. 7.

Comparison of the headgroup area at the lipid–water interface in these PEs shows that the values of A are considerably larger and increase more rapidly with an increase in temperature in the L$_\alpha$ phase than in the H$_{II}$ phase. However, at temperatures just below and just above the T_h, the values of A in both the L$_\alpha$ phase and the H$_{II}$ phase are largely independent of hydrocarbon chain structure. These results indicate that, although differences in hydrocarbon chain structure may determine the T_h on the absolute temperature scale by virtue of differences in the rate of hydrocarbon chain shortening, the structure of the hydrocarbon chains probably makes only a small contribution to the limiting area per molecule at the lipid–water interface in both the L$_\alpha$ and H$_{II}$ phases of these PEs. An overview of the $\langle l \rangle$ and A data suggests that these two parameters are in direct competition, with the decreasing lipid length driving the lipid–water interface to larger and larger areas in the L$_\alpha$ phase. Eventually, the lamellar morphology becomes too costly energetically, and the system is forced to adopt the H$_{II}$ phase, where the extra degree of geometric freedom allows both the hydrocarbon chains and polar headgroups to assume their desired states.

The following picture is suggested as an explanation for this behavior (Tate and Gruner, 1989). There are two main free energies in the system, one driving the hydrocarbon chains to a desired length that decreases with increasing temperature and the other free energy pushing the headgroup to an optimum area that is relatively temperature independent. In the L$_\alpha$ phase (for a nearly constant molecular volume), the lipid length and headgroup area at the lipid–water interface are uniquely related (see Eq. 10). Hence, these two free energies are in direct competition, with the decreasing lipid length and concomitant splaying of the hydrocarbon chains driving the lipid–water interface to larger and larger areas. Eventually, this becomes too costly and the system is forced into the H$_{II}$ phase, where the extra degree of geometric freedom allows both the hydrocarbon chains and headgroups to assume (on average) their desired states. The only free energy cost keeping the system out of the H$_{II}$ phase is that the lipid hydrocarbon chains are forced to assume a variety of lengths to fill the hexagon (see Fig. 6). This free energy cost due to the packing of the lipid chains in the H$_{II}$ phase was demonstrated by Kirk et al. (1984).

These observations will be extended in another paper to be presented elsewhere by considering lipids with a similar

spectrum of hydrocarbon chain structures but different chain lengths and polar headgroups (D. A. Mannock, R. N. A. H. Lewis, R. N. McElhaney, P. E. Harper, and S. M. Gruner, submitted for publication).

REFERENCES

American Petroleum Institute Research Project 44, Carnegie Institute, Pittsburgh, PA. Princeton University Annex.

Harper, P. E. 1996. Structural Studies of Surfactant and Polymer Systems. Ph.D. thesis. Dept. of Physics, Princeton University, Princeton, NJ.

Harper, P. E., and S. M. Gruner. 2000. Electron density modeling and reconstruction of infinite periodic minimal systems (IPMS) based phases in lipid–water systems I. Modeling IPMS based phases. *Eur. Phys. J. E.* 2:217–228.

Harper, P. E., S. M. Gruner, R. N. A. H. Lewis, and R. N. McElhaney. 2000. Electron density modeling and reconstruction of infinite periodic minimal systems (IPMS) based phases in lipid–water systems II. Reconstruction of D-surface based phases. *Eur. Phys. J. E.* 2:229–245.

Kirk, G. L., S. M. Gruner, and D. L. Stein. 1984. A thermodynamic model of the lamellar (L_α) to inverse hexagonal (H_{II}) phase transition of lipid membrane–water systems. *Biochemistry.* 23:1093–1102.

Lewis, R. N. A. H., D. A. Mannock, R. N. McElhaney, D. C. Turner, and S. M. Gruner. 1989. The effect of fatty acid chain length and structure on the lamellar gel to liquid–crystalline and lamellar to reversed hexagonal phase transitions of aqueous phosphatidylethanolamine dispersions. *Biochemistry.* 28:541–548.

Mariani, P., E. Rivas, V. Luzzati, and H. Delacroix. 1990. Polymorphism of a lipid extract from *Pseudomonas fluorescens*: structure analysis of a hexagonal phase and of a novel cubic phase of extinction symbol Fd$--$. *Biochemistry.* 29:6799–6810.

Melchior, D. L., F. J. Scavitto, and J. M. Steim. 1980. Dilatometry of dipalmitoyllecithin-cholesterol bilayers. *Biochemistry.* 19:4828–4834.

Nagle, J. F., and D. Wilkinson. 1978. Lecithin bilayers. *Biophys. J.* 23:159–179.

Stamatoff, J. B., and S. Krimm. 1976. Phase determination of x-ray reflections for membrane-type systems with constant fluid density. *Biophys. J.* 16:503–516.

So, P. T. C. 1992. High Pressure Effects on the Mesophases of Lipid–Water Systems. Ph.D. thesis. Dept. of Physics, Princeton University, Princeton, NJ.

So, P. T. C., S. M. Gruner, and E. Shyamsunder. 1992. Automated pressure and temperature control apparatus for x-ray powder diffraction studies. *Rev. Sci. Instr.* 63:1763–1770.

So, P. T. C., S. M. Gruner, and E. Shyamsunder. 1993. Pressure induced topological phase transitions in membranes. *Phys. Rev. Lett.* 70:3455–3458.

Tate, M. W., and S. M. Gruner. 1989. Temperature dependence of the structural dimensions of the inverted hexagonal (H_{II}) phase of phosphatidylethanolamine containing membranes. *Biochemistry.* 28:4245–4253.

Tate, M. W., S. M. Gruner, and E. F. Eikenberry. 1997. Coupling format variations in x-ray detectors based on charge coupled devices. *Rev. Sci. Instr.* 68:47–54.

Turner, D. C. 1990. Structural Investigations of the Inverted Hexagonal and Inverted Cubic Phases in Lipid–Water Systems. Ph.D. thesis. Dept. of Physics, Princeton University, Princeton, NJ.

Turner, D. C., and S. M. Gruner. 1992. X-ray diffraction reconstruction of the inverted hexagonal (H_{II}) phase in lipid–water systems. *Biochemistry.* 31:1340–1355.

Vand, V., A. Aitken, and R. K. Campbell. 1949. Crystal structure of silver salts of fatty acids. *Acta Cryst.* 2:398–403.

Warren, B. E. 1969. X-ray Diffraction. Addison-Wesley, Reading, MA.

Weast, R. C. editor. 1975. Handbook of Chemistry and Physics, 55th edition. CRC Press, Boca Raton, FL.

Wiener, M. C., G. I. King, and S. H. White. 1992. Structure of a fluid dioleoylphosphatidylcholine bilayer determined by a joint refinement of x-ray and neutron diffraction data. III. Complete structure. *Biophys. J.* 61:434–447.

Yang, C. P., M. C. Wiener, R. N. A. H. Lewis, R. N. McElhaney, and J. F. Nagle. 1986. Dilatometric studies of isobranched phosphatidylcholines. *Biochim. Biophys. Acta.* 863:33–44.